JACS
JOURNAL OF THE AMERICAN CHEMICAL SOCIETY
Article
pubs.acs.org/JACS

Using Self-Organization To Control Morphology in Molecular Photovoltaics

Seok Ju Kang,[†,#] Seokhoon Ahn,[†,#] Jong Bok Kim,[‡] Christine Schenck,[†] Anna M. Hiszpanski,[‡] Seokjoon Oh,[†] Theanne Schiros,[§] Yueh-Lin Loo,[‡] and Colin Nuckolls*[,†]

[†]Department of Chemistry and [§]Columbia Energy Frontier Research Center (EFRC), Columbia University, New York, New York 10027, United States

[‡]Department of Chemical and Biological Engineering, Princeton University, Princeton, New Jersey 08544, United States

Supporting Information

ABSTRACT: This work explores the formation of well-defined molecular *p*−*n* junctions in solution-processed self-assembled heterojunction solar cells using dodecyloxy-substituted contorted hexabenzocoronene (12-*c*-HBC) as a donor material and phenyl-C_{70}-butyric acid methyl ester ($PC_{70}BM$) as an acceptor. We find that the contorted 12-*c*-HBC molecules effectively assemble in solution to form a nested structure with the ball-shaped $PC_{70}BM$. The result is a self-assembled molecular-scale *p*−*n* junction. When this well-defined *p*−*n* junction is embedded in active films, we can make efficient self-assembled solar cells with minimal amounts of donor material relative to the acceptor. The power conversion efficiency is drastically enhanced by the mode of donor and acceptor assembly within the film.

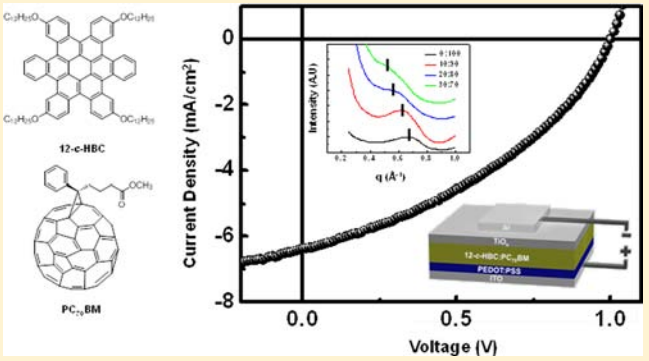

INTRODUCTION

Here we describe a self-assembly process between an electron donor and an electron acceptor in solution that controls the morphology in thin-film solar cells. A general understanding of how to control morphology in organic photovoltaics (OPVs) is needed to spur progress in solar cell optimization.[1,2] The interpenetrating network of polymer donor materials and fullerene derivatives has been shown to increase the efficiency in polymer solar cells.[3,4] Moreover, self-assembly of donors and acceptors in polymer bulk heterojunction solar cells has been proposed to further control the molecular-scale structure and increase the efficiency.[5−8] For molecularly based solar cell morphology, the task is all the more difficult because often the donor and acceptor are created independently of each other and have no obvious modes of interaction and assembly. Our strategy is to create donor and acceptor materials with complementary shapes to encourage their assembly. Using this strategy, we can create a well-defined interface between donor and acceptor and study this assembly in the context of photovoltaic devices. The remarkable finding from this study is that the stoichiometry between donor and acceptor controls a hierarchy of self-assembly that is responsible for the overall film morphology. Maximum performance of photovoltaic devices is observed at the optimized ratio of the two semiconductors. This ratio uses very small amounts of the electron donor relative to the electron acceptor (≤10 wt% ≈ 8 mol%!).

The molecules studied here are a dodecyloxy-substituted contorted hexabenzocoronene (12-*c*-HBC)[9] and a soluble fullerene ($PC_{70}BM$),[1] shown in Figure 1. The structure of the hexabenzocoronene is doubly concave due to the steric

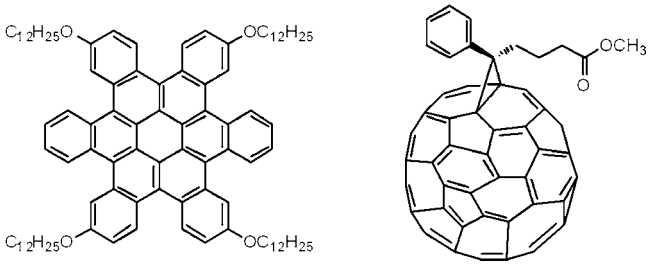

Figure 1. Chemical structures of contorted 12-*c*-HBC and $PC_{70}BM$ molecule.

congestion at the periphery of the molecule.[9] The six benzylated rings fold up and down around the exterior of the molecule. We have observed assembly of the unsubstituted version of this molecule and the closely related thienyl versions of these molecules with C_{60} and C_{70}.[10,11] We observe assembly in co-crystals and at interfaces with the concave faces of the donor nesting with the convex surface of the fullerenes. Other

Received: September 2, 2012
Published: January 30, 2013

examples of specific interactions between fullerene and aromatic compounds include "buckyclutchers" [12−15] and other bowl-shaped aromatics.[9,16] The structural and electronic complementarity of the molecules at the donor and acceptor interface controls device performance.[17] Here, we study together for the first time the soluble versions of both the 12-*c*-HBC and the fullerene and monitor their assembly in films from solution.

RESULTS AND DISCUSSION

Figure 2 shows grazing incidence X-ray diffraction (GIXD) measurements from spin-cast films with varying ratios of donor

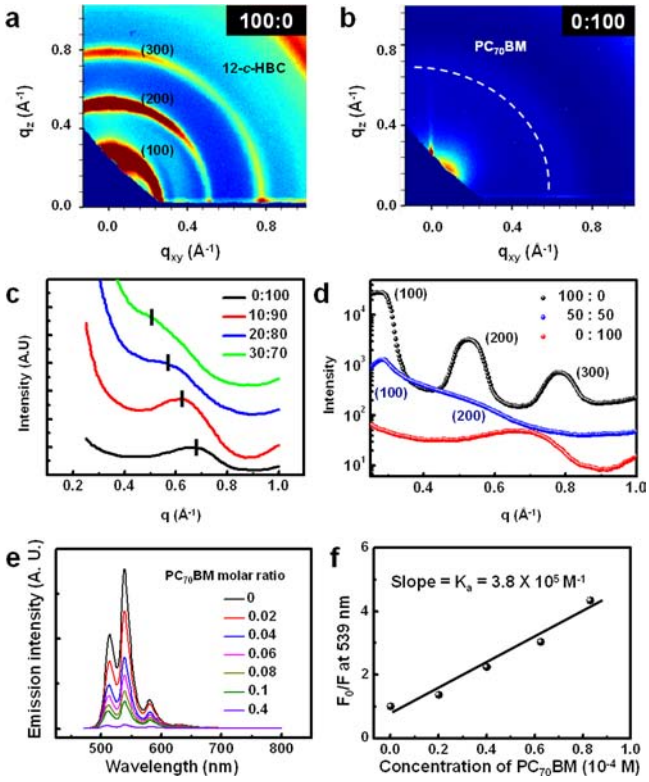

Figure 2. 2D GIXD pattern for (a) 12-*c*-HBC and (b) $PC_{70}BM$. (c,d) Intensity profiles along the 60° diagonal direction as a function of donor:acceptor blend ratio. (e) Fluorescence quenching with $PC_{70}BM$ for 12-*c*-HBC. (f) Stern−Volmer plots of 12-*c*-HBC as a function of $PC_{70}BM$ concentration.

and acceptor. To understand the packing motif from the mixture of donor and acceptor, films from pure donor and acceptor were also investigated. The 2-D GIXD pattern in Figure 2a shows the cross-sectional planes of the pure 12-*c*-HBC film. The two-fold symmetry reveals the existence of a preferred orientation in the 12-*c*-HBC crystal in the film. Previous single-crystal diffraction of 12-*c*-HBC reveals that it packs in a monoclinic structure with unit cell parameters of a = 2.44 nm, b = 1.97 nm, and c = 0.874 nm.[18] In the GIXD, there are three strong meridian reflections at q_z = 0.26, 0.52, and 0.77 $Å^{-1}$, corresponding to the (100), (200), and (300) reflections of a 12-*c*-HBC crystalline lattice. The orientation of the a axis is preferentially aligned perpendicular to the substrate, indicating that the disk-shaped molecule is oriented edge-on to the substrate.

The GIXD pattern of $PC_{70}BM$ shows the weak, broad intensity from a $PC_{70}BM$ thin-film layer at q_z = 0.67 $Å^{-1}$.[17,19] The short-range ordered $PC_{70}BM$ is due to the fast spin-coating process that reduces the reflection's intensity in the GIXD measurement.[20]

In blended films of 12-*c*-HBC and $PC_{70}BM$, the high flux of the synchrotron X-ray source allows us to observe the change in q value of 12-*c*-HBC and $PC_{70}BM$ diffractions in the blend film as a function of donor:acceptor ratio. The q value of 12-*c*-HBC and $PC_{70}BM$ blend films decreases monotonically from 0.68 to 0.58 $Å^{-1}$ as the 12-*c*-HBC weight fraction increases up to 20%, as depicted in the 1-D line cut in Figure 2c. However, the origin of the shoulder at q = 0.52 $Å^{-1}$ in the 30:70 ratio blend (12-*c*-HBC:$PC_{70}BM$) is ambiguous because the q = 0.52 $Å^{-1}$ is overlapping with the second-order diffraction of pure 12-*c*-HBC film. It is surprising that only 10% of 12-*c*-HBC changes the overall q value in the film. A plausible explanation for this is that assembly between donor and acceptor occurs. For the donor values below 10%, we could not observe a change in the q value from the GIXD pattern due to the small amount of the co-crystal, but we speculate the assembly also occurs based on the increased solar cell performance (*vide infra*). This observation is consistent with the expectation that a ball-and-socket type interaction between 12-*c*-HBC and $PC_{70}BM$ molecules should increase the overall d-spacing of $PC_{70}BM$ in the film. In other words, if the 12-*c*-HBC molecules were self-aggregating in the $PC_{70}BM$ medium, the q value in the GIXD pattern from pure $PC_{70}BM$ would remain unchanged. We conclude from these data that at ∼10% 12-*c*-HBC in $PC_{70}BM$, the molecules self-organize into a new nested structure in the films. Furthermore, fluorescence quenching of the photoluminescence experiment supports our claim. We found a significant amount of association between 12-*c*-HBC and $PC_{70}BM$ in *o*-xylene solvent (Figure 2e,f).

For the blend films with over 40% 12-*c*-HBC, the GIXD pattern shows two strong diffractions corresponding to the (100) and (200) reflections of the 12-*c*-HBC crystal (see Figure 2d). This clearly indicates that the film is beginning to macro-phase-segregate at high ratios of 12-*c*-HBC relative to $PC_{70}BM$. $PC_{70}BM$ intensity is not observed in the GIXD pattern of blend films over 40% 12-*c*-HBC, indicating that no microdomain exists of $PC_{70}BM$ that can be detected by GIXD. The absence of $PC_{70}BM$ reflections in our film is likely due to the high crystallinity of 12-*c*-HBC obscuring the weaker $PC_{70}BM$ diffraction.

Although the GIXD results suggested the formation of donor−acceptor complex in blend films, the packing structure of the complex was still ambiguous. To investigate this packing motif of the donor−acceptor complex, the self-assembly behavior from the mixture of 12-*c*-HBC and $PC_{70}BM$ was examined using transmission electron microscopy (TEM) on the microcrystals grown by slow solvent evaporation of the blend solutions from *o*-xylene on an amorphous carbon-coated TEM grid. To compare assembly behavior observed in blend films with microcrystals from the mixture, the crystallization was monitored as a function of donor:acceptor ratio.

For pure $PC_{70}BM$, the selected area electron diffraction (SAED) pattern of the microcrystal of $PC_{70}BM$ shows a hexagonal symmetry (a = b = 1.05 nm, c = 2.47 nm), as can be seen in Figure 3a. The first diffraction spot can be distinguished with a d-spacing of 0.87 nm. The bc-plane of $PC_{70}BM$ crystal is observed normal to the electron beam, which is consistent with other studies.[21] For pure 12-*c*-HBC, the diffraction pattern of the microcrystal from the bc-plane is well characterized with series of spot reflections as shown in Figure 3b. The SAED

dx.doi.org/10.1021/ja308628z | J. Am. Chem. Soc. 2013, 135, 2207−2212

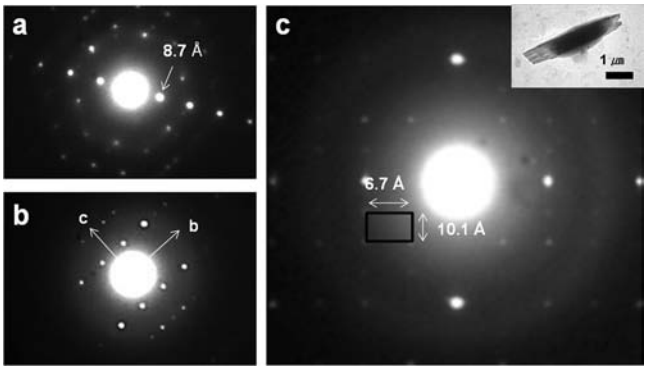

Figure 3. Bright-field TEM micrographs of (a) $PC_{70}BM$ and (b) 12-*c*-HBC microcrystal; insets show their SAED patterns. (c) SAED pattern of co-crystal and bright-field image (inset).

pattern exhibits a set of (0*kl*) reflections indexed with lattice constants of a monoclinic structure of 12-*c*-HBC crystals (a = 2.44 nm, b = 1.97 nm, c = 0.874 nm, and β = 96.98°) that is well matched with not only the expected [100] projection of 12-*c*-HBC[18] but also the GIXD pattern of the (*h*00) reflections shown in Figure 2a.

In a complementary set of experiments, we grew microcrystals from the mixed solutions by slow evaporation of the solvent as a function of donor:acceptor ratio. Three different types of reflections were detected by SAED in the 10/90 to 30/70 wt% 12-*c*-HBC/$PC_{70}BM$ samples. We observed pure 12-*c*-HBC, pure $PC_{70}BM$, and a new type of diffraction shown in Figure 3c (see also Supporting Information, Figure S1). When the 12-*c*-HBC ratio was over 40%, the new type of crystal was not observed, and only pure 12-*c*-HBC or pure $PC_{70}BM$ diffraction could be seen. We speculate that the new diffraction pattern that is distinct from that of either pure 12-*c*-HBC or $PC_{70}BM$ is from a co-crystal of 12-*c*-HBC and $PC_{70}BM$. The self-assembly behavior observed in the microcrystals from the mixtures was similar to that observed in films, although the ratios were slightly different. The difference in ratios is presumably due to the different growth conditions.

The common observation between the GIXD on films and the SAED on microcrystals is that the complex formation of 12-*c*-HBC and $PC_{70}BM$ occurs with small amounts (10−30 wt%) of 12-*c*-HBC. Phase segregation of 12-*c*-HBC and $PC_{70}BM$ occurs above 40 wt% of 12-*c*-HBC. This result indicates that the same packing motif of 12-*c*-HBC and $PC_{70}BM$ observed in the microcrystal is adopted in films with 10−30 wt% 12-*c*-HBC. Thus, understanding the structure in the microcrystal of this donor−acceptor complex provides important information to understand the structure in active films of OPVs.

In Figure 3c, the representative series of reflections from the new crystalline form in the microcrystals is observed near 0.67 and 1.01 nm, respectively. To understand the structure of this new type of diffraction pattern, we first compared this pattern with the co-crystal structure of unsubstitued *c*-HBC and C_{60}. Previously, we observed single co-crystal formation for C_{60} and unsubstituted *c*-HBC in a ball-and-socket motif grown by physical vapor deposition (PVD).[10] Although the structure of *c*-HBC and C_{60} is different than the present case, we expected that a 12-*c*-HBC/$PC_{70}BM$ blend system follows the same packing motif as *c*-HBC and C_{60}. For the *c*-HBC/C_{60} co-crystal, the space group is monoclinic $c2/m$, and the unit cell lattice parameters are a = 2.23 nm, b = 1.62 nm, c = 1.58 nm, α = 90.00°, β = 95.87°, and γ = 90.00°. The co-crystal has an ABAB packing structure while forming continuous channels of *c*-HBC and C_{60} perpendicular to the surface. The distance from the center of C_{60} to the next *c*-HBC is 0.67 nm in the *c*-HBC/C_{60} co-crystal system.[10] This 0.67 nm reflection is also observed in the orthotropic diffraction pattern of the microcrystal seen in Figure 3c. Thus, we can expect that the new type of crystal also has an ABAB packing structure with continuous channels of 12-*c*-HBC and $PC_{70}BM$ normal to the surface.

To further understand this new type of diffraction pattern, we analyzed the diffraction after tilting the same microcrystal in the TEM.[22] The sample was tilted by 30° from its original position along the meridian, and a new Bragg reflection from a plane in the microcrystal was observed, as shown in in Figure 4b. The *d*-spacing of the rectangular diffraction pattern in the

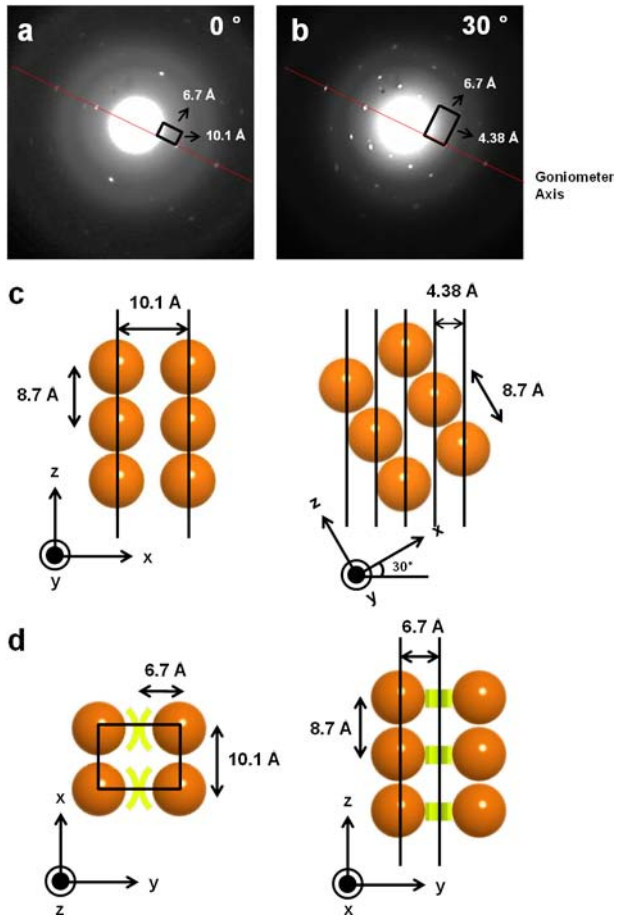

Figure 4. SAED patterns of $PC_{70}BM$ and 12-*c*-HBC co-crystal (a) at 0° and (b) after 30° tilting. (c) Schematic model showing the relationship between co-crystal structure and electron diffraction at 0° and after 30° tilting. (d) Proposed model of the intermolecular *p*−*n* junction crystal structure.

tilted sample is 0.67 and 0.44 nm, respectively. The *d*-spacing of 0.44 nm is clearly obtained all over the Ewald sphere. This 0.44 nm distance from the diffraction pattern is the same as the center-to-center distance of $PC_{70}BM$ of 0.87 nm before tilting 30°, as shown in Figure 4c.[21] This result also indicates that 12-*c*-HBC and $PC_{70}BM$ form continuous channels perpendicular to the surface with ABAB packing.

From these results, we can create a model of the co-crystal as shown schematically in Figure 4d. The contorted 12-*c*-HBC molecules are stacked between $PC_{70}BM$ molecules with ball-

dx.doi.org/10.1021/ja308628z | J. Am. Chem. Soc. 2013, 135, 2207−2212

and-socket packing motif while keeping their own channels perpendicular to the substrate. We hypothesize that this packing motif is adopted in the films as well, resulting in well-defined molecular $p-n$ junctions with their own channels perpendicular to the substrate. The device performance in OPVs, as discussed below, also supports this claim.

Figure 5 shows the device properties for the self-assembled material in a solution-processed solar cell. We used a TiO_x layer

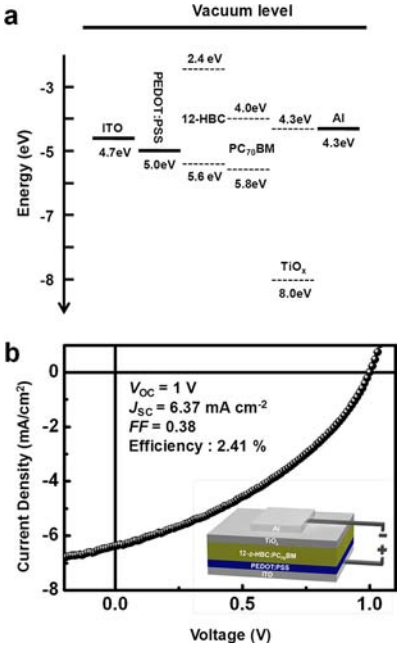

Figure 5. (a) Energy level diagram of the device. (b) $J-V$ characteristics of a 10/90 wt% 12-*c*-HBC/$PC_{70}BM$ device under light illumination.

(Figure 5a) because, when inserted between an active film and a top Al electrode, it acts as an optical spacer and protects the organic active film from humidity and oxygen.[23−25] The solar cell device of 10/90 wt% 12-*c*-HBC/$PC_{70}BM$ shows 2.41% efficiency with an open circuit voltage (V_{OC}) of 1 V,[26] a short-circuit current (J_{SC}) of 6.37 mA cm^{-2}, and a fill factor (FF) of 0.38. The efficiency of 2.41% is much higher than that of the corresponding bilayer solar cell[10] and occurs despite the highest external quantum efficiency absorption range of 12-*c*-HBC/$PC_{70}BM$ being around ∼400 nm (Figure S2).

To understand the role of the molecular $p-n$ junction in the solar cell, we made photovoltaics as a function of blend ratio to mirror the structural studies described above. The solar cell performances of these films were measured with the device architecture as shown in Figure 6a. The solar cell consists of a

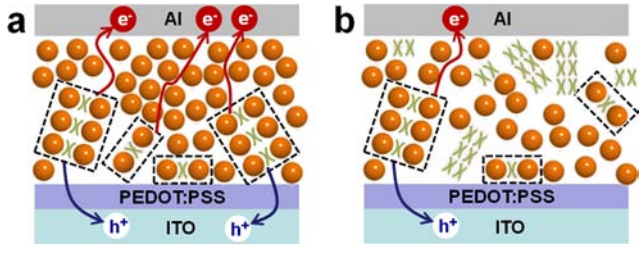

Figure 6. Schematic model of the intermolecular $p-n$ junction assembly in the $PC_{70}BM$ medium at (a) 10/90 and (b) 30/70 wt%.

70 nm thick 12-*c*-HBC/$PC_{70}BM$ fil-spin coated on a layer of PEDOT:PSS, followed by thermal evaporation of 60 nm thick Al as a top contact. We measure the solar cells using a Keithley 2635 source measurement unit under AM 1.5G 100 mW/cm^2 illumination. The device performance with 10/90 wt% 12-*c*-HBC/$PC_{70}BM$ shows V_{OC} = 0.97 ± 0.03 V, J_{SC} = 5 ± 0.3 mA cm^{-2}, and FF = 0.35 ± 0.02, resulting in a power conversion efficiency (PCE) of 1.69 ± 0.2% across 30 devices. The PCE of 12-*c*-HBC/$PC_{70}BM$ solar cell films exponentially decreases with the increase of the 12-*c*-HBC fraction in the film, as depicted in Figure 7b. The dramatic decrease of efficiency at 30/70 wt%

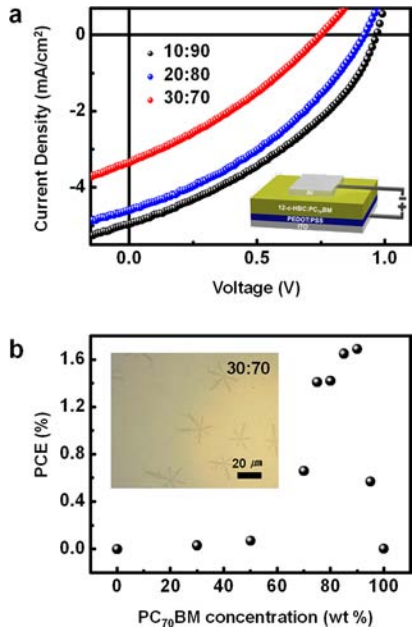

Figure 7. (a) $J-V$ curves of ITO/PEDOT:PSS/12-*c*-HBC:$C_{70}BM$/Al architecture solar cells as a function of blend ratio. (b) Plots of average PCE of solar cell as a function of the amount of the $PC_{70}BM$ content in the film; inset displays optical microscopy image of 30/70 wt% 12-*c*-HBC/$PC_{70}BM$ blend ratio film.

12-*c*-HBC/$PC_{70}BM$ can be explained on the basis of phase separation caused by aggregation of donor molecules into a pure 12-*c*-HBC domain, as illustrated schematically in Figure 6 and seen experimentally in the optical microscopy image in the inset to Figure 7b.

The striking feature of the data in Figure 7 is the factor of 600 increase in device efficiency on going from a pure $PC_{70}BM$ solar cell with an efficiency of ∼0.003% to a film that has only 10% of the donor material. This dramatic enhancement supports the formation of well-defined intermolecular $p-n$ junctions, as depicted in Figure 6, that play a critical role in controlling the morphology of the film and the conversion efficiency.[27,28] We further reduced the donor ratio in the solution to confirm the existence of intermolecular $p-n$ junctions. We fabricated a 5/95 wt% 12-*c*-HBC/$PC_{70}BM$ solar cell, and it shows higher solar efficiency (∼0.6%) than that of the pure $PC_{70}BM$ solar cell. It also should be noted that we observe the highest solar cell performance at ratios from 10/90 to 30/70 wt% 12-*c*-HBC/$PC_{70}BM$. This range is where we observe the formation of donor−acceptor complexes in films and in the microcrystals. The relationship between device performance and packing structure in films supports the formation of the complex.

dx.doi.org/10.1021/ja308628z | J. Am. Chem. Soc. 2013, 135, 2207−2212

Further evidence of the formation of a well-defined molecular *p*−*n* junction in the film can be obtained through thermal annealing[29,30] or using additives[31,32] that destroy or hinder the association between the donor and acceptor. 12-*c*-HBC has two transition temperatures at 91 and 285 °C, which correspond to the transition to the liquid crystalline mesophase and to the isotropic liquid, repectively.[9] Heating above the liquid crystalline mesophase transition temperature (91 °C) destroys the heteromolecular assembly and encourages columnar assembly. After the 10/90 wt% 12-*c*-HBC/$PC_{70}BM$ film was heated to 150 °C for 10 min and then cooled to room temperature, the device performance eroded sharply (Figure 8a). The optical micrograph of the post-annealing films shows

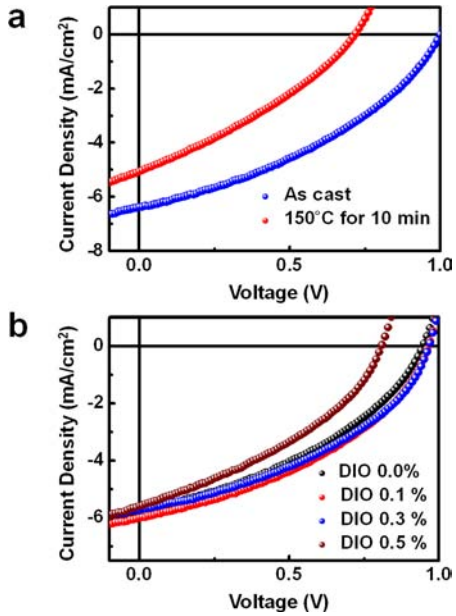

Figure 8. (a) *J*−*V* curves of ITO/PEDOT:PSS/12-*c*-HBC:$PC_{70}BM$/TiO_x/Al architecture solar cells. The thermally annealed sample exhibits a decreased efficiency. (b) *J*−*V* curves of a solar cell as a function of DIO ratio in the solution.

evidence of phase separation (Figure S3a,b). To hinder the formation of a *p*−*n* junction, 1,8-diiodooctane (DIO) was used as an additive because DIO has a higher boiling point than that of *o*-xylene and good affinity to $PC_{70}BM$.[31] The *p*−*n* junction formation between 12-*c*-HBC and $PC_{70}BM$ can be interrupted when DIO is present. This expectation was matched with the device performance. The PCE of 10/90 wt% 12-c-HBC/$PC_{70}BM$ film decreased as the DIO fraction increased up to 0.5% (Figure 8b). These two experimental results demonstrate the importance of assembly between 12-*c*-HBC and $PC_{70}BM$ through ball-and-socket interactions to increase the area of the *p*−*n* junction and increase efficiency in solar cells.

CONCLUSIONS

In summary, a molecular-scale *p*−*n* junction is formed by self-assembly in a solution-processed solar cell. Only 10% of donor material is required to achieve the maximum power conversion efficiency of 2.41%, which is high considering the absorption profile of the 12-*c*-HBC molecule is largely confined to the UV range. These results reveal that non-covalent interactions between a contorted discotic donor and a ball-shape $PC_{70}BM$ are a viable design strategy for solution-processed solar cells.

ASSOCIATED CONTENT

Supporting Information

Experimental details, fluorescence and UV−visible spectra, GIXD plot, SAED pattern, and EQE data. This material is available free of charge via the Internet at http://pubs.acs.org.

AUTHOR INFORMATION

Corresponding Author

cn37@columbia.edu

Author Contributions

#S.J.K. and S.A. contributed equally.

Notes

The authors declare no competing financial interest.

ACKNOWLEDGMENTS

This research was supported by the U.S. Department of Energy through the EFRC program (Grant DE-SC0001085) and the FENA (Grant 2009-NT-2048). J.B.K. and Y.-L.L. also acknowledge funding by the Photovoltaics Program at ONR (N00014-11-10328) and an NSF-sponsored MRSEC through the Princeton Center for Complex Materials (DMR-0819860). A.M.H. was supported by the U.S. Department of Defense through the National Defense Science & Engineering Graduate Fellowship Program. C.S. is supported by the National Science Foundation Graduate Research Fellowship under award no. DGE-1144155. Portions of this research were carried out at Beamline 11-3 at the Stanford Synchrotron Radiation Lightsource, a national user facility operated by Stanford University on behalf of the U.S. Department of Energy, Office of Basic Energy Sciences which is supported by the U.S. Department of Energy, Office of Basic Energy Sciences, under Contract No. DE-AC02-98CH10886.

REFERENCES

(1) Gunes, S.; Neugebauer, H.; Sariciftci, N. S. *Chem. Rev.* **2007**, *107*, 1324−1338.
(2) Venkataraman, D.; Yurt, S.; Venkatraman, B. H.; Gavvalapalli, N. *J. Phys. Chem. Lett.* **2010**, *1*, 947−958.
(3) Yu, G.; Gao, J.; Hummelen, J. C.; Wudi, F.; Heeger, A. J. *Science* **1995**, *270*, 1789−1791.
(4) Halls, J. J. M.; Walsh, C. A.; Greenham, N. C.; Marseglia, E. A.; Friend, R. H.; Moratti, S. C.; Holmes, A. B. *Nature* **1995**, *376*, 498−500.
(5) Mayer, A. C.; Toney, M. F.; Scully, S. R.; Rivnay, J.; Brabec, C. J.; Scharber, M.; Koppe, M.; McCulloch, I.; McGehee, M. *Adv. Funct. Mater.* **2009**, *19*, 1173−1179.
(6) Miller, N. C.; Sweetnam, S.; Hoke, E. T.; Gysel, R.; Miller, C. E.; Bartelt, J. A.; Xie, X.; Toney, M. F.; McGehee, M. D. *Nano Lett.* **2012**, *12*, 1566−1570.
(7) Cates, N. C.; Gysel, R.; Beiley, Z.; Miller, C. E.; Toney, M. F.; Heeney, M.; McCulloch, I.; McGehee, M. D. *Nano Lett.* **2009**, *9*, 4153−4157.
(8) Kennedy, R.; Ayzner, A. L.; Wanger, D. D.; Day, C. T.; Halim, M.; Khan, S. I.; Tolbert, S. H.; Schwartz, B. J.; Rubin, Y. *J. Am. Chem. Soc.* **2008**, *130*, 17290−17292.
(9) Xiao, S.; Myers, M.; Miao, Q.; Sanaur, S.; Pang, K.; Steigerwald, M. L.; Nuckolls, C. *Angew. Chem., Int. Ed.* **2005**, *44*, 7390−7394.
(10) Tremblay, N. J.; Gorodetsky, A. A.; Cox, M. P.; Schiros, T.; Kim, B.; Steiner, R.; Bullard, Z.; Sattler, A.; So, W.-Y.; Itoh, Y.; Toney, M. F.; Ogasawara, H.; Ramirez, A. P.; Kymissis, I.; Steigerwald, M. L.; Nuckolls, C. *ChemPhysChem* **2010**, *11*, 799−803.
(11) Chiu, C.-Y.; Kim, B.; Gorodetsky, A. A.; Sattler, W.; Wei, S.; Sattler, A.; Steigerwald, M.; Nuckolls, C. *Chem. Sci.* **2011**, *2*, 1480−1486.
(12) Rabideau, P. W.; Sygula, A. *Acc. Chem. Res.* **1996**, *29*, 235−242.

(13) Sygula, A.; Fronczek, F. R.; Sygula, R.; Rabideau, P. W.; Olmstead, M. M. *J. Am. Chem. Soc.* **2007**, *129*, 3842−3843.
(14) Georghiou, P. E.; Dawe, L. N.; Tran, H. A.; Strube, J.; Neumann, B.; Stammler, H.-G.; Kuck, D. *J. Org. Chem.* **2008**, *73*, 9040.B.. Stammler, H.-G.; Kuck, D. *J. Org. Chem.* **2008**, *73*, 9040−9047.
(15) Zhong, Z.-L.; Ikeda, A.; Shinkai, S. *Calixarenes*; Kluwer Academic Publishers: Dordrecht, 2001; pp 476−495.
(16) Bharat; Bhola, R.; Bally, T.; Valente, A.; Cyrański, M. K.; Dobrzycki, Ł.; Spain, S. M.; Rempała, P.; Chin, M. R.; King, B. T. *Angew. Chem., Int. Ed.* **2010**, *49*, 399−402.
(17) Kang, S. J; Kim, J. B.; Chiu, C.-Y.; Ahn, S.; Schiros, T.; Lee, S. S.; Yager, K. G.; Toney, M. F.; Loo, Y. L.; Nuckolls, C. *Angew. Chem., Int. Ed.* **2012**, *51*, 8594−8597.
(18) Harris, K. D.; Xiao, S.; Lee, C. Y.; Strano, M. S.; Nuckolls, C.; Blanchet, G. B. *J. Phys. Chem. C* **2007**, *111*, 17947−17951.
(19) Verploegen, E.; Mondal, R.; Bettinger, J. C.; Sok, S.; Toney, F. M.; Zhenan, B. *Adv. Funct. Mater.* **2010**, *20*, 3519−3529.
(20) Yang, X. N.; van Duren, J. K. J.; Rispens, M. T.; Hummelen, J. C.; Janssen, R. A. J.; Michels, M. A. J.; Loos, J. *Adv. Mater.* **2004**, *16*, 802−806.
(21) Zheng, L. D.; Han, Y. C. *J. Phys. Chem. B* **2012**, *116*, 1598−1604.
(22) Park, Y. J.; Kang, S. J.; Lotz, B.; Brinkmann, M.; Thierry, A.; Kim, K. J.; Park, C. *Macromolecules* **2008**, *41*, 8648−8654.
(23) Kim, J. Y.; Kim, S. H.; Lee, H. H.; Lee, K.; Ma, W. L.; Gong, X.; Heeger, A. J. *Adv. Mater.* **2006**, *18*, 572−576.
(24) Kim, C. S.; Lee, S. S.; Gomez, E. D.; Kim, J. B.; Loo, Y. L. *Appl. Phys. Lett.* **2009**, *94*, 113302.
(25) Park, S. H.; Roy, A.; Beaupre, S.; Cho, S.; Coates, N.; Moon, J. S.; Moses, D.; Leclerc, M.; Lee, K.; Heeger, A. J. *Nat. Photonics* **2009**, *3*, 297−302.
(26) Brabec, C. J.; Cravino, A.; Meissner, D.; Sariciftci, N. S.; Fromherz, T.; Minse, M.; Sanchez, L.; Hummelen, J. C. *Adv. Funct. Mater.* **2001**, *11*, 374−380.
(27) Wang, H.; Shah, M.; Ganesan, V.; Chabinyc, M. L.; Loo, Y. L. *Adv. Energy Mater.* **2012**, *2*, 1447−1455.
(28) Wang, H.; Gomez, E. D.; Kim, J.; Guan, Z.; Jaye, C.; Fischer, D. A.; Kahn, A.; Loo, Y.-L. *Chem. Mater.* **2011**, *23*, 2020−2023.
(29) Dang, M. T.; Hirsch, L.; Wantz, G. *Adv. Mater.* **2011**, *23*, 3597−3602.
(30) Li, G.; Shrotriya, V.; Huang, J.; Yao, Y.; Moriarty, T.; Emery, K.; Yang, Y. *Nat. Mater.* **2005**, *4*, 864−868.
(31) Lee, J. K.; Ma, W. L.; Brabec, C. J.; Yuen, J.; Moon, J. S.; Kim, J. Y.; Lee, K.; Bazan, G. C.; Heeger, A. J. *J. Am. Chem. Soc.* **2008**, *130*, 3619−3623.
(32) Yao, Y.; Hou, J. H.; Xu, Z.; Li, G.; Yang, Y. *Adv. Funct. Mater.* **2008**, *18*, 1783−1789.